Gamma irradiation synthesis and *in vitro* drug release studies of ZnO/PVA hydrogel nanocomposites

Swaroop Kumaraswamy[1], Gangadhar Babaladimath[2], Vishalakshi Badalamoole[2], Somashekarappa H Mallaiah[1]*

[1]*Centre for Application of Radioisotopes and Radiation Technology (CARRT), Mangalore University, Mangalagangotri 574199, Karnataka, India*
[2]*Department of Post-Graduate Studies & Research in Chemistry, Mangalore University, Mangalagangothri 574 199, Karnataka, India*

*Corresponding author, Tel: (+91) 824-2284545; E-mail: carrtmu@gmail.com

Abstract

In the present work, the synthesis of ZnO/PVA hydrogel nanocomposites was carried out using the gamma irradiation technique. The ZnO nanoparticles were synthesized using co-precipitation method and dispersed in the PVA solution. To prepare the ZnO/PVA hydrogel nanocomposites, the mixture was exposed to gamma irradiation dose of 25 kGy. The formation of ZnO nanoparticles in PVA matrix was confirmed using the powder X-ray diffraction (XRD), Fourier Transform Infrared Spectroscopy (FTIR), and the UV-Visible Spectrophotometer (UV). The surface morphology of the hydrogels was studied using the Field Emission Scanning Electron Microscopy (FESEM). The swelling ratio and equilibrium degree of swelling (% EDS) were evaluated and there was drastic reduction in swelling and % EDS with the addition of ZnO nanoparticles to the PVA mixture. The l-ascorbic acid was loaded to the hydrogels and the release data was monitored by the absorption wavelength at 252 nm using UV. The drug release data was fitted to zero order, first order, Higuchi's model, and Korsmeyer-Peppas's model for the detailed analysis. The results suggest that ascorbic acid release from the hydrogel matrix follows the non-Fickian mechanism. Copyright © 2017 VBRI Press.

Keywords: Gamma irradiation; l-ascorbic acid; drug release; XRD; FESEM.

Introduction

Hydrogels are the three dimensional polymer networks which have generated great interest by the researchers in recent years because of their biocompatibility with blood, body fluids, and tissues [1-3]. Hydrogels are able to retain large amount of water or any biological fluids within its network [4, 5]. Due to these distinctive properties, it is used in wound care, drug delivery, dental materials, tissue engineering, injectable polymeric system, cosmetic products and many other applications [6-8]. The development of nanoparticles enforced hydrogels has gained attention in the biomedical field because of its distinctive physicochemical properties, versatile adaptation potential and multifuctionalities [9, 10]. The application of PVA has been well documented in biotechnology and biomedicine due to its superior mechanical properties, chemical resistance, biocompatibility, long term temperature and pH stability and hydrophilic nature [11, 12]. PVA is also a good host material for metal and semiconductor nanomaterials due to its thermo-stability, good capping ability, and gel forming abilities [12]. Studies on inorganic based nanocomposite hydrogels are very relevant and promising in biomedical and pharmaceutical research because of their great potential to inhibit microbial growth. Zinc oxide (ZnO) is an inorganic semiconductor material with a rich variety of configuration compared to any other known nanomaterial [13]. ZnO nanoparticles, in recent years, have emerged as a good antimicrobial agent because of its abundant functionality, biocompatibility, excellent resistance to sterilization, good efficacy over several microbial species, and low cost. For hydrogel synthesis, irradiation with gamma radiation or electron beam is the preferred method of synthesis over other conventional chemical and physical methods because it modifies as well as sterilizes the material in a single step, which is its distinctive feature [14]. Moreover, radiation synthesis does not involve any chemical initiators and cross-linking agents for the material modification process and hence retains the biocompatibility of materials specifically used in biomedical applications [15]. L-ascorbic acid (Vitamin-C) is a powerful antioxidant

which safeguards the body cells from damage and is a common ingredient in skin care products and helps in a variety of metabolic ways [16].

In vitro drug release testing is a vital investigative tool that is used to establish product behaviour during various phases of the drug product development. It reveals essential information on dosage form and its behaviour, as well as details on release mechanism and kinetics. These are essential in the scientific approach to drug product development. In the present study, an attempt was made to synthesise the ZnO/PVA hydrogel nanocomposite using gamma irradiation technique followed by *in vitro* release studies of l-ascorbic acid from the synthesized hydrogels.

Experimental

Materials

Synthesis of ZnO was carried out using zinc nitrate hexahydrate [$Zn(NO)_3.6H_2O$] ($\geq$ 99 %) and sodium hydroxide [NaOH] ($\geq$ 97 %) procured form Merck, Mumbai, India. The hydrogel were synthesized using poly (vinyl alcohol) ($\geq$ 99 %) procured from Sigma Aldirich, USA. L-ascorbic acid ($\geq$ 99%) was procured from Merck, Mumbai, India. All the chemicals were of analytical grade and used without further purification. Double distilled quality of water (resistivity: >5 MΩ. cm at 25^0 C) was used throughout the experiment. The gamma irradiation was performed using the gamma irradiator (GC-5000, BRIT, Mumbai, India) loaded with cobalt-60 (^{60}Co) source which delivers a dose rate of 5.9 kGy/h.

Synthesis of ZnO nanoparticle, pure PVA hydrogel, and ZnO/PVA hydrogel nanocomposites

ZnO nanoparticles were prepared by the co-precipitation method. The synthetic procedure involved drop-wise addition of 0.2 M NaOH to 0.1 M $Zn(NO)_3.6H_2O$ under stirring at room temperature. The precipitate so obtained was washed thrice with double distilled water to remove the impurities. The powder obtained was dried in a hot air oven at 110^0 C for 6 hours and used for the preparation of the PVA nanocomposites.

The PVA stock solution was prepared by dissolving weight of 5% PVA in double distilled water at 80^0 C under constant stirring until a the homogenous mixture was obtained. Further different weight percentages of the prepared ZnO nanoparticles, namely, 0% (PVA), 1% (PZ1), 2% (PZ2), and 3% (PZ3) were added to the PVA stock solution separately. Each composition was sonicated for about 15 minute for proper and uniform dispersion of the ZnO nanoparticles in the PVA solution. The solution was bubbled with argon gas in air sealed container to remove the O_2 content. Pure PVA and the PVA/ZnO mixture were transferred into separate glass container of dimension 10 cm x 10 cm x 0.4 cm. All the samples were subjected to gamma irradiation of 25 kGy at a dose rate of 5.9 kGy/h at room temperature for cross-linking of the PVA matrix as well as for the entrapment of the ZnO nanoparticles in the PVA matrix. The hydrogels were cut into cylindrical disks and dried at room temperature.

Characterization

The optical characterization of the synthesised hydrogels was carried out using the Ultraviolet-Visible (UV) spectrophotometer (UV-2600, Shimadzu, Japan) within a scan range of 200 to 800 nm. The powder X-ray diffraction measurements for the samples were recorded using the X- ray diffractometer (Miniflex, Rigaku, USA) over a diffraction angle (2θ) range set from 10° to 80° at a scan rate of 3°/min to perform structural analysis. The average crystallite size 'D' of all the samples was calculated using the first approximation of the Debye-Schrrer equation (1).

$$D = \frac{0.9\lambda}{\beta \cos\theta} \qquad (1)$$

where, 'D' is the average crystallite size of the particles, λ is the wavelength of the X-rays, β is the full width half maxima of the maximum intensity peak, and θ is the diffraction angle. Crystallinity of a polymer material is one of the most important aspects for mechanically analyzing the material. Percentage crystallinity of a polymer material can be measured by equation (2) using the XRD spectra

$$\% \, crystallinity = \frac{total\ area\ of\ the\ crystalline\ peaks}{total\ area\ of\ all\ peaks} \, X \, 100 \qquad (2)$$

The average intercrystallite separation 'R' in the amorphous region of the polymer samples was estimated using equation (3).

$$R = \frac{5\lambda}{8\sin\theta} \qquad (3)$$

The functional groups present in the samples were studied using the Fourier Transform Infrared (FTIR) spectrometer (Prestige-21, Shimardzu, Japan). The surface morphological properties of the synthesised hydrogels were evaluated using the Field Emission Scanning Electron Microscopy (FESEM) (ULTRA 55 FESEM, Karl Zeiss, Germany).

Swelling studies

In order to study the swelling behavior, the dried hydrogel samples were cut into portion of 2 cm^2 of approximately 1 g weight (W_i). The hydrogel samples were immersed in water at room temperature and taken out at periodic intervals 't'; the surface water was removed by smoothly wiping the hydrogel with filter paper and weighed (W_f). The percentage swelling (%S) of the hydrogel samples was measured at predetermined times up to 72 hours using equation (4).

$$\%S = \frac{W_f - W_i}{W_i} X100 \qquad (4)$$

The equilibrium degree of swelling (% EDS) was calculated using equation (5) at the maximum swollen state of the hydrogel.

$$\% EDS = \frac{W_\infty - W_o}{W_o} \times 100$$

(5)

where, 'W_o' is the weight of the dried hydrogel and 'W_∞' is the swollen hydrogel at saturation state.

Drug release kinetics

The dried samples were immersed in the ascorbic acid solution in the absence of light until equilibrium swelling was achieved (72 hours). The swollen samples were kept for drying at room temperature for 24 hours, followed by placing it in a hot air oven at 45^0 C until it dried completely. No change in color was observed in the ascorbic acid stock solution as well as in the loaded hydrogels indicating no oxidation of l-ascorbic acid during the loading process. The amount of drug loaded was estimated using the calibration curve. The calibration curve was plotted with a freshly prepared solution of ascorbic acid (lowest of 1 mg to highest of 6 mg of ascorbic acid in 100 ml of double distilled water). The calibration curve was linear with a correlation coefficient $R^2 = 0.98$. The drug release kinetics of the hydrogels was studied using the Dissolution tester (Electrolab TDT-08L). The measurement of the ascorbic acid release was carried out using the UV-Visible spectrophotometer at an absorbance wavelength of 252 nm. To study the drug release kinetics, the loaded hydrogels were continuously stirred at 100 rpm in double distilled water at room temperature. In order to follow the drug release kinetics, the absorbance of the solution was measured at different time intervals up to 72 hours. The drug dissolving medium was replaced with fresh double distilled water after every subsequent sample to maintain constant volume. The cumulative drug released (CDR) at different intervals of time was calculated using equation (7).

$$\% CDR = \frac{The\ amount\ of\ drug\ released\ from\ the\ gel}{The\ amount\ of\ drug\ loaded\ to\ the\ gel} X100$$

(7)

The kinetics of drug released was studied using the zero order, first order, Higuchi's model, and Korsmeyer-Peppas's model. The equations are given below:

The zero order equation (8) explains the systems in which the drug release rate is independent of its concentration [17]. To study the zero order drug release kinetics the data of percentage cumulative drug released (%CDR) was plotted against time.

Zero order kinetics: $F = k_0 t$ (8)

where 'F' is the fraction of drug released at time't' and k_0 is the drug release constant for zero order.

Concentration dependent release rate of the systems can be explained using the first order equation (9) [18]. For first order drug release kinetics studies the data obtained was plotted as log of cumulative percentage of drug remained versus time.

First order kinetics: $\log C_0 - \log C = \frac{k_1 t}{2.303}$ (9)

where, C_0 and C are the concentration of drug remained at time zero and at time 't' and 'k_1'is the drug release constant for first order.

Higuchi's model describes the drug release from the insoluble matrix system as a square root of time dependent process based on Fick's law. This system can be used to describe the drug dissolution from several types of modified release pharmaceutical dosage forms like, transdermal systems and matrix tablets with water soluble drugs. In general, Higuchi's model in its simplest form can be expressed by equation (10) [17].

Higuchi's model: $F = k_H t^{1/2}$ (10)

where, 'F' is the fraction of drug released at time't' and 'k_H' is Higuchi's dissolution constant.

The Korsmeyer-Peppas's model describes the drug release rate from a polymeric system. To study the drug release mechanism 60 % of the release data was fitted in equation (11). To study the release kinetics, the data obtained from the *in vitro* drug release studies was plotted as log %CDR versus log time.

Korsmeyer-Peppas's model: $\frac{M_t}{M_\infty} = kt^n$ (11)

where, 'M_t/M_∞' is the fraction of drug release at time't'. 'k' is the constant incorporating structural and geometric characteristics of the drug dosage form and 'n' is the drug release exponent which explains the drug release mechanism. In Korsmeyer-Peppas's model, the value of 'n' differentiates the release mechanism of the drug. For the case of cylindrical samples, $0.45 \leq n$ corresponds to a Fickian diffusion mechanism, $0.45 < n < 0.89$ to a non-Fickian transport, $n = 0.89$ to case II (relaxational) transport, and $n > 0.89$ to super case II transport [17].
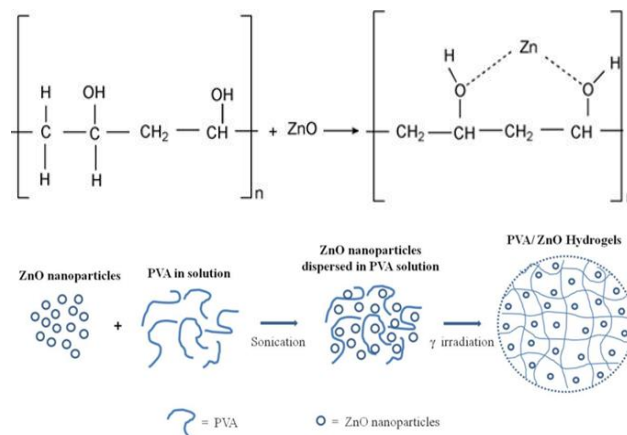
Fig. 1. (a) Chemical reaction between PVA and ZnO nanoparticles and (b) Schematic representation of ZnO/PVA hydrogel nanocomposite synthesis using gamma irradiation technique.

Results and discussion

Fig. 1 shows the possible chemical reaction and schematic representation of immobilization of the ZnO nanoparticles in the PVA matrix. The ZnO nanoparticles were dispersed in 5 wt% PVA solution using sonication which was further irradiated by 25 kGy gamma radiation. The irradiation brings about cross-linking in the PVA matrix resulting in the formation of ZnO/PVA hydrogel nanocomposites. The localization of the ZnO nanoparticles within the gel network is visually identified by its uniform pale whitish appearance.
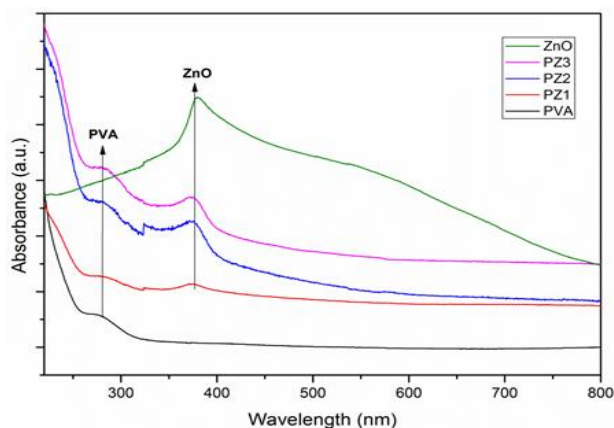
Fig. 2. UV-visible spectra of pure PVA, ZnO nanoparticles, and ZnO/PVA hydrogel nanocomposites.

The formation of ZnO nanoparticles in the PVA network was identified by analyzing the UV spectrum. UV spectroscopic analysis is primarily effective in confirming the presence of nanoparticles in the UV region as well as in the visible region. **Fig. 2** illustrates the absorption spectrum of ZnO/PVA hydrogel nanocomposites. Since ZnO is a transparent semiconductor, the absorption edge is observed in the UV region (~373 nm) including the PVA characteristic peak at 260 nm for all combination of the ZnO/PVA hydrogels confirming the entrapment of ZnO nanoparticles in the PVA network. Significant improvement in absorption intensity was observed for PZ2 and PZ3 at 373nm due to higher concentration of ZnO nanoparticles entrapped in PVA network.

The FTIR analysis **(Fig. 3)** was performed to understand the possible interaction between the ZnO nanoparticles and the PVA hydrogel matrix. The FTIR spectra were taken over a wavenumber range of 4000 to 400 cm^{-1} for pure PVA as well as for different composites of the ZnO/PVA hydrogels. A broad absorption band was observed at ~3000-3600 cm^{-1} representing the O-H stretching vibration of the PVA. Bands discernible at 2920 and 2850 cm^{-1} were assigned to CH and CH_2 asymmetric stretching vibrations of PVA. A weak peak at 1740 cm^{-1} representing the C=O stretching vibration corresponded to the vinyl acetate group of the PVA. A strong vibration peak at 1640 cm^{-1} corresponded to the C=C stretching of the PVA. The peak at 1537 cm^{-1} present only in the ZnO/PVA hydrogel nanocomposites

are attributed to the C=O stretching corresponding to the metal acetate bonding. A strong band at 1091 cm^{-1} recognized as C-O stretching mode of the PVA diminished in the ZnO/PVA hydrogels due to the defects induced by the ZnO nanoparticles. The band observed at 840 cm^{-1} in the PVA sample attributed to the C-C stretching was affected and shifted to the lower wave number at 825 cm^{-1} for ZnO/PVA hydrogel nanocomposites. Further, the peak observed at 459 cm^{-1} in the ZnO/PVA hydrogel nanocomposite attributed to the Zn-O stretching validated the presence of ZnO in PVA complex. Symmetric shift in wave number, appearance of new peaks, and variation in the intensities of the peak in the FTIR spectra of the ZnO/PVA hydrogel nanocomposites in comparison to the pure PVA spectra represent specific interaction in the hydrogel network.
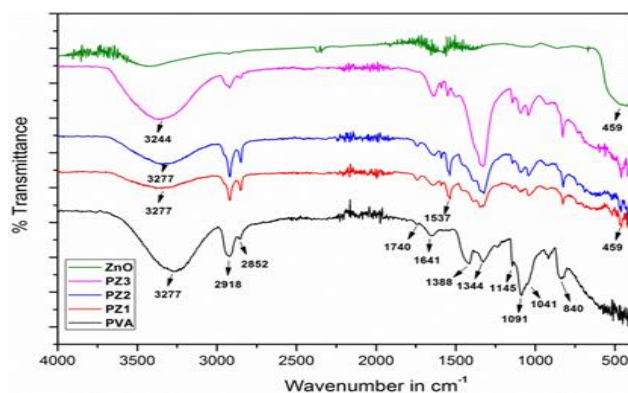
Fig. 3. FTIR spectra of pure PVA, ZnO nanoparticles, and ZnO/PVA complexes.

Pure PVA, pure ZnO nanopowder, and ZnO/PVA hydrogel nanocomposites were analyzed with powder X-ray diffraction to study the nature of crystallinity of the samples. The powder X-ray diffraction pattern of the ZnO/PVA hydrogels was compared with the pure PVA hydrogel and ZnO nanopowder in **Fig. (4).** A broad intense peak appeared in the PVA, and the PVA/ZnO nanocomposites at the scattering angle of $2\theta = \sim19^0$ related to the 'd' spacing of 4.57 Å can be matched to the (101) reflection plane of the crystalline PVA **[19, 20]**. The crystalline nature of PVA can be attributed to the strong interaction between the PVA chains through intermolecular hydrogen bonding. The X-ray diffraction pattern of the ZnO nanoparticles describes the hexagonal wurtzite structure. In ZnO/PVA hydrogels, the crystalline peaks appeared at $2\theta = 31.68°, 34.04°, 35.5°, 48.12°, 56.76°, 63.52°, 65.92°,$ and $68.4°$ pertaining to the hexagonal phase of zinc oxide **[21, 22]** along with the PVA characteristic peak at 19°, indicating the presence of ZnO nanoparticles in the PVA network. The intensity of the ZnO crystalline peaks were less in the PZ1 and PZ2 samples. This may be due to the lesser concentration of ZnO in the PVA matrix. The average crystallite size 'D', percentage crystallinity, and average inter crystallite separation 'R' of all the samples are tabulated in **Table 1**. Crystallite size 'D' is observed to increase in the crystallite size with ZnO concentration. It was also

observed that the percentage crystallinity of the samples steeply increases with increase in the ZnO concentration. These observations show changes in the structural uniformity of the main chain of the polymeric matrix, formed due to the coordination oxygen ions of ZnO with the hydroxyl group of the PVA network.
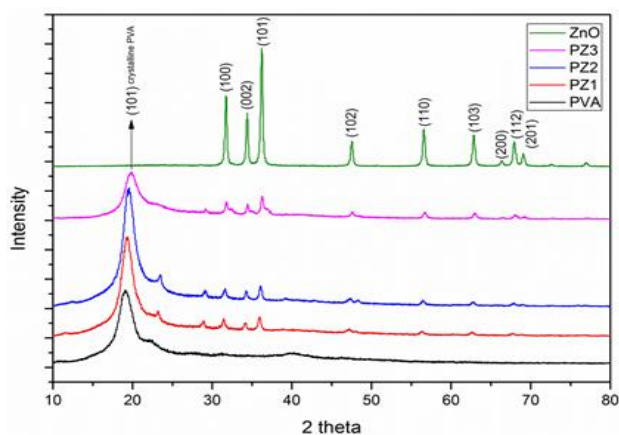
Fig. 4. XRD spectra of pure PVA, ZnO nanoparticles, and ZnO/PVA hydrogel nanocomposites.

The surface morphological changes occurring in the PVA hydrogels on incorporation of the ZnO nanoparticles has been investigated by FESEM analysis. **Fig. (5)** shows the surface morphology of pure PVA, ZnO, and the three ZnO/PVA hydrogel nanocomposite samples. Pure PVA hydrogel **[Fig. 5(a)]** possess a smooth surface with no traces of break and agglomeration. Pure ZnO nanoparticles **[Fig. 5(b)]** exhibit flake like structures. The magnified view of the ZnO/PVA nanocomposite sample **[Fig. 5(c)]** resembles the flake like ZnO nanostructures on the surface of the PVA matrix with a tendency to agglomerate. **Fig. 5 (d-f)** demonstrates morphology of the PVA/ZnO hydrogel nanocomposites with different amount of ZnO concentration (1 - 3 wt %). It shows the appearance of aggregated and randomly distributed ZnO nanoparticles on top of PVA surface. An increase in the distribution of the ZnO nanoparticles in the PVA matrix was observed with the increase in the ZnO concentration.

Fig. (6) shows the influence of ZnO concentration on swelling behavior of ZnO/PVA hydrogels. A drastic decrease in % swelling was observed for ZnO/PVA hydrogel when compared to pure PVA hydrogel. With the increasing concentration of ZnO in the ZnO/PVA hydrogels, the %swelling shows a slight decrease.
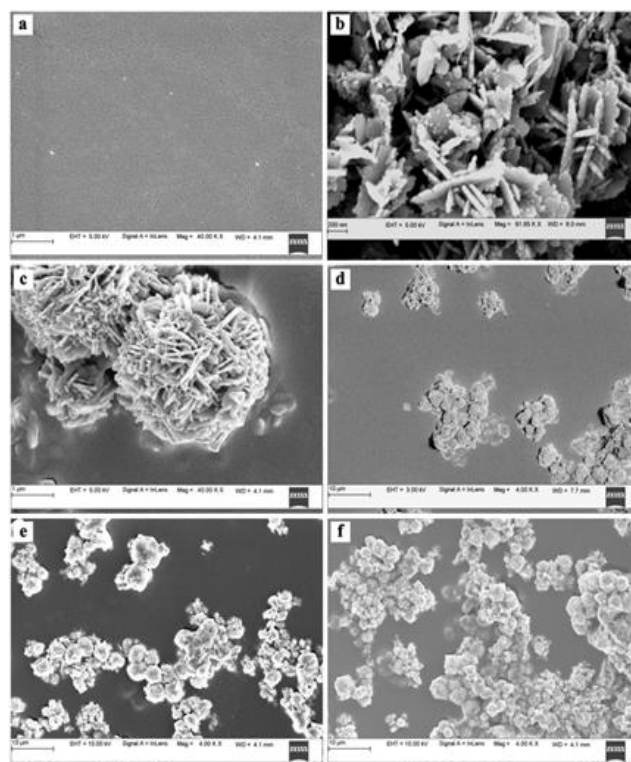
Fig. 5. FESEM images of (a) Pure PVA hydrogel, (b) ZnO nanoparticles prepared by co-precipitation method, (c) Magnified image of ZnO/PVA hydrogel nanocomposite, (d) PZ1, (e) PZ2, and (f) PZ3.
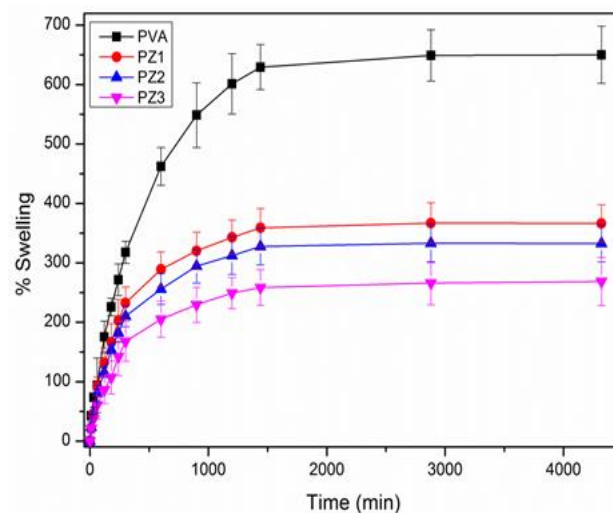
Fig. 6. Swelling of PVA and ZnO/PVA hydrogel nanocomposites.

Table 1. Percentage composition, average crystallite size 'D', % crystallinity, intercrystalline separation 'R', % Equilibrium Degree of Swelling, and % Gel Fraction of pure PVA, ZnO nanoparticles, and ZnO/PVA complexes.

Sample	Composition	'D' in nm	% crystallinity	'R' in Å	% EDS	% GF
ZnO	Pure ZnO	26 for (101) ZnO crystalline peak	--	--	--	--
PVA	Pure PVA	3.8	62.9	5.80	650	84
PZ1	PVA/1% ZnO	4.4	70.26	5.68	366	73
PZ2	PVA/2% ZnO	4.8	73.5	5.77	333	72
PZ3	PVA/3% ZnO	5.0	77.1	5.60	265	69

The samples immersed in the double distilled water reach equilibrium degree of swelling when the water uptake and elastic force of the cross-linking reaches equilibrium. All the samples attain equilibrium swelling at 24 hours. The % EDS was calculated for all the samples immersed in distilled water for 24 hours using equation (5) and the results are listed in **Table 1**. The observed decrease in the swelling capacity of the PVA/ZnO hydrogels may be because of the decrement of hydrophilicity of the hydrogels network with addition of ZnO nanoparticles due to involvement of –OH groups of PVA in bonding with ZnO nanoparticles.

The gel fraction (%GF) of all the samples was evaluated using equation (6) to find quantitative cross-linking percentage of the hydrogesls. The results are tabulated in **Table 1**. The PVA hydrogel showed the highest % GF in comparison with the PVA/ZnO hydrogels. The % GF of the PVA/ZnO hydrogels showed a decreasing trend with increasing ZnO concentration.

Since decrease in the % EDS in the PVA/ZnO hydrogel nanocomposites was observed with increase in the ZnO concentration, PZ1 was selected for the drug release studies on the basis of the highest %EDS among all the composites. To understand the l-ascorbic acid release from the hydrogel, *in vitro* drug release experiments were carried out on PVA and PZ1 hydrogels at room temperature. The percentage cumulative drug release (%CDR) was calculated for both the hydrogels using equation (7).

Fig. 7. Drug release data for pure PVA and PZ1 hydrogel nanocomposite (a) Zero order plot, (b) First order plot, (c) Higuchi's model, and (d) Korsmeyer-Peppas's model.

Fig. 7(a) displays the %CDR profile of both the hydrogels. The % CDR is slightly higher in the case of PVA compared to the PZ1 hydrogel. To explain the kinetics of release of ascorbic acid from the PVA and PZ1 hydrogels, the drug release data of both the hydrogels were fit into zero order, first order, Higuchi's model, and Korsmeyer-Peppas's model (**Fig. 7**). The selection of the most suitable model for drug release kinetics was based on the idyllic fit indicated by the value of correlation coefficient 'R^2' close to unity. In both the hydrogels the 'R^2' value for first order release was found to be higher in comparison with the zero order indicating that the release rate is concentration dependent [18]. In Higuchi's model the plot of %CDR versus the square root of time is linear indicating diffusion controlled system. The drug release mechanism of both the hydrogels was established by fitting the first 60% of the release data in the Korsmeyer-Peppas's model. The value of diffusion exponent 'n' was established form the slope of the plot log (M_t/M_∞) versus log t. Since the value of 'n' obtained for both the hydrogels was between 0.45 and 0.89 the release mechanism was considered to be non-Fickian or anomalous in nature [17].

Conclusion

In this paper, gamma radiation assisted synthesis of PVA hydrogel and ZnO/PVA hydrogel has been reported. The ZnO nanoparticles embedded PVA gel was characterized using UV, FTIR, XRD, and FESEM techniques. The UV analysis of the ZnO/PVA hydrogels exhibits a strong absorption peak at ~373 nm along with the PVA characteristic peak at ~260 nm confirming the existence of ZnO nanoparticles in the PVA matrix. The functional group modifications and the presence of Zn-O stretching vibrations at ~460 cm^{-1} observed from the FTIR analysis explains the possible interaction of the ZnO/PVA composites. XRD confirms the formation of ZnO/PVA hydrogel nanocomposites by means of increasing crystallite size 'D' and % crystallinity with ZnO concentration. The FESEM images of the ZnO/PVA complexes expose the presence of morphological structures of the ZnO nanoparticles distributed randomly on the surface of the PVA matrix. Remarkable decrease in % EDS was observed in the ZnO/PVA hydrogel nanocomposites in comparison with pure PVA hydrogel, attributed to the interaction of the ZnO nanoparticles with the hydroxyl group of the PVA. This was also evident from a significant decrease in swelling of the hydrogel

Table 2. Interpretation of different drug release kinetic models and diffusion mechanism for pure PVA and PZ1 hydrogel nanocomposite.

Drug loaded sample code	Correlation coefficient (R^2) values				Diffusion exponent 'n'	Mechanism of release
	Zero order	First order	Higuchi's model	Korsmeyer-Peppas's model		
PVA	0.73	0.98	0.95	0.98	0.71	non-Fickian
PZ1	0.76	0.98	0.96	0.99	0.69	non-Fickian

nanocomposites. L-ascorbic acid was loaded on pure PVA and PZ1 hydrogels and the release kinetics was studied. The drug release data was best fitted to Korsemeyer-Peppas's model and the release exponent 'n' indicated the non-Fickian nature of drug release in both the hydrogels.

Author's contributions

[1]Swaroop K.: Performed all the experiment and wrote the paper.
[2]Gangadhar B.: Performed the experiments for the drug release studies.
[2]Vishalakshi B.: Analysed FTIR and drug release data.
[1]Somashekarappa H. M.: Conceived the plan and analysed all the data.

References

1. Klein, A.; Whitten, P.G.; Resch, K.; Pinter, G.; *J. Polym. Sci., Part B: Polym. Phys.*, **2015**, *53*, 1763.
   DOI: 10.1002/polb.23912
2. Atul Tiwari, Ashutosh Tiwari (Eds), Bioengineered Nanomaterials, CRC Press, USA, **2013**.
3. Jonker, A.M.; Bode, S.A.; Kusters, A.H.; Van Hest, J.C.M.; Lowik, D.W.P.M.; *Macromol. Biosci.*, **2015**, *15*, 1338–1347.
   DOI: 10.1002/mabi.201500110
4. Rashmi, K.; Dibyendu, S.B.; Indra, N.; *Adv. Mater. Lett.*, **2013**, *5*, 214.
   DOI: 10.5185/amlett.2013.8541
5. Kumari, A.; Kaith, B.S.; Singha, A.S.; Kaliac, S.; *Adv. Mater. Lett.*, **2010**, *1*, 123.
   DOI: 10.5185/amlett.2010.6129
6. Polu, A.R.; Kumar, R.; Kumar, K.V.; *Adv. Mater. Lett.*, **2012**, *3*, 406.
   DOI: 10.5185/amlett.2011.6375
7. Fiamingo, A.; Montembault, A.; Boitard, S.E.; Naemetalla, H.; Agbulut, O.; Delair, T.; *Biomacromolecules.*, **2016**, *17*,1662.
   DOI: 10.1021/acs.biomac.6b00075
8. Zakaria, A.S.; Afifi, S.A.; Elkhodairy, K.A.; *BioMed Res. Int.*, **2016**, *2016*, 1.
   DOI: 10.1155/2016/6525163
9. Gaharwar, A.K.; Peppas, N.A.; Khademhosseini, A.; *Biotechnol. Bioeng.*, **2014**, *111*, 441.
   DOI: 10.1002/bit.25160.
10. Hossein, O.; Kinam, P. Fundamentals and Applications of Controlled Release Drug Delivery; Siepmann, J.; Ronald, S.; Michael, R. (Eds.); Springer: New York, **2012**, pp. 75-106.
    DOI: 10.1007/978-1-4614-0881-9_4.
11. Lim, K.S.; Roberts, J.J.; Alves, M.H.; Poole-Warren, L.A.; Martens, P.J.; *J. Appl. Polym. Sci.*, **2015**, *132*, 42142.
    DOI: 10.1002/app.42142
12. Oliveira, R.N.; McGuinness, G.B.; Rouze, R.; Quilty, B.; Cahill, P.; Soares, G.D.A.; Thire, R.M.S.M.; *J. Appl. Polym. Sci.*, **2015**, *132*, 42129.
    DOI: 10.1002/app.42129
13. Chand, P.; Gaur, A.; Kumar, A.; *Adv. Mater. Lett.*, **2013**, *4*, 220–224.
    DOI: 10.5185/amlett.2012.7391
14. Francis, S.; Mitra, D.; Dhanawade, B.R.; Varshney, L.; Sabharwal, S.; *Radiat. Phys. Chem.*, **2009**, *78*, 951.
    DOI: 10.1016/j.radphyschem.2009.07.020
15. Abd El-Mohdy, H.L.; *J. Polym. Res.*, **2013**, *20*, 177.
    DOI: 10.1007/s10965-013-0177-6
16. Mangir, N.; Bullock, A.J.; Roman, S.; Osman, N.; Chapple, C.; MacNeil, S.; *Acta Biomater.*, **2016**, *29*, 188.
    DOI: 10.1016/j.actbio.2015.10.019
17. Costa, P.; Lobo, J.M.; *Eur. J. Pharm. Sci.*, **2001**, *13*, 123.
    DOI: 10.1016/S0928-0987(01)00095-1
18. Dash, S.; Murthy, P.N.; Nath, L.; Chowdhury, P.; *Acta Pol. Pharm.*, **2010**, *67*, 217.
    DOI: 10.1016/S0928-0987(01)00095-1
19. Gupta, S.; Webster, T.J.; Sinha, A.; *J. Mater. Sci. Mater. Med.*, **2011**, *22*, 1763.
    DOI: 10.1007/s10856-011-4343-2
20. Kumar, A; Negi, Y.S.; Bhardwaj, N.K.; Choudhary, V.; *Adv. Mater. Lett.*, **2013**, *4*, 626.
    DOI: 10.5185/amlett.2012.12482
21. Singh, R.P.; Shukla, V.K.; Yadav, R.S.; Sharma, P.K.; Singh, P.K.; Pandey, A.C.; *Adv. Mater. Lett.*, **2011**, *2*, 313.
    DOI: 10.5185/amlett.indias.204
22. Kondawar, S.B.; Acharya, S.A.; Dhakate, S.R.; *Adv. Mater. Lett.*, **2011**, *2*, 362.
    DOI: 10.5185/amlett.2011.9107am2011
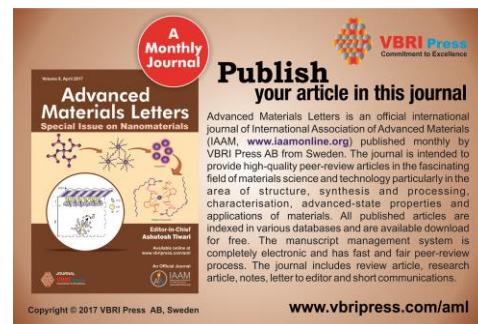
Supplementary information

a)   Chemical reactions
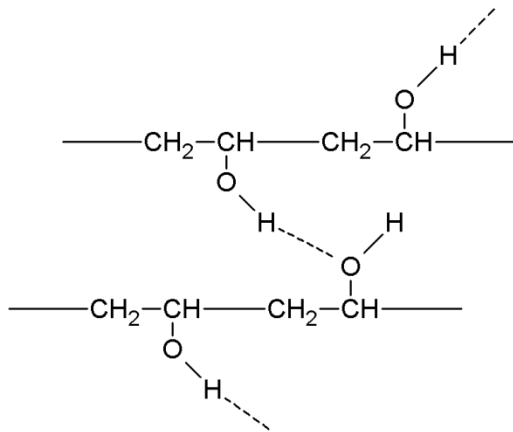
Fig. Inermolecular hydrogen bonding of PVA.

b) Digital photographs:

Fig. PVA and ZnO/PVA hydrogel nanocomposites.